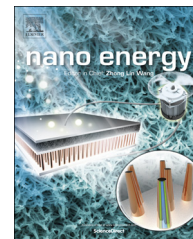




Available online at www.sciencedirect.com

ScienceDirect

journal homepage: www.elsevier.com/locate/nanoenergy



RAPID COMMUNICATION

Coupled optical and electrical modeling of thin-film amorphous silicon solar cells based on nanodent plasmonic substrates



Ruichao Guo^{a,b}, Hongtao Huang^{a,b}, Paichun Chang^c, Linfeng Lu^b, Xiaoyuan Chen^b, Xiaofei Yang^a, Zhiyong Fan^{d,*}, Benpeng Zhu^{a,e,**}, Dongdong Li^{b,***}

^aSchool of Optical and Electronic Information, Huazhong University of Science and Technology, Wuhan 430074, China

^bShanghai Advanced Research Institute, Chinese Academy of Sciences, 99 Haik Road, Zhangjiang Hi-Tech Park, Pudong, Shanghai 201210, China

^cDepartment of Creative Industry, Kainan University, Kainan University, No. 1, Kainan Road, Luchu, Taoyuan County 338, Taiwan

^dDepartment of Electronic and Computer Engineering, Hong Kong University of Science and Technology, Clear Water Bay, Kowloon, Hong Kong, China

^eState Key Laboratories of Transducer Technology, Shanghai Institute of Microsystem and Information Technology, Chinese Academy of Sciences, Shanghai 200050, China

Received 1 May 2014; accepted 28 May 2014

Available online 13 June 2014

KEYWORDS

Thin-film amorphous silicon solar cell;
Surface plasmon resonance;
Optical and electrical simulation;
Local current reversal

Abstract

Advanced light managements on nanostructured substrates have delivered outstanding optical absorption enhancement for high performance solar cells. In this work, thin-film amorphous silicon (*a*-Si:H) solar cell with efficient light trapping capability was constructed on the nano-patterned back reflector. In order to investigate the fundamental properties of the nano-patterned solar cell, the spatial distributions of electrical properties in silicon absorption layers are simulated by a coupled optical and electrical modeling method. The current density and electric field distribution under different bias voltages are compared. While the patterned device shows much higher short circuit current density, the open circuit voltage (V_{OC}) is lower than its counterpart. In nanostructured device, the relatively weak electric field is preferred to

*Corresponding author.

**Corresponding author at: School of Optical and Electronic Information, Huazhong University of Science and Technology, Wuhan 430074, China.

***Corresponding author.

E-mail addresses: eezf@ust.hk (Z. Fan), benpengzhu@mail.hust.edu.cn (B. Zhu), lidd@sari.ac.cn (D. Li).

be localized in the top corners, where a local current reversal will occur and lead to the reduction of V_{OC} . An increasing doping concentration in p -layer promotes the internal electric field as well as the corresponding short circuit current and open circuit voltage. This work provides guidelines for rational design of light harvesting nanostructure for high performance thin film solar cells.

© 2014 Elsevier Ltd. All rights reserved.

Introduction

Thin film solar cells are highly attractive solutions for flexible and low cost solar energy conversion. Advanced light management strategies based on nano-structures have been developed in order to explore the full potential of thin-film solar cells [1-5]. Rather than the conventional randomly micron-sized textured substrates [6,7], three-dimensional (3-D) nanostructures, such as nanopillars [1], nanocones [2,8], nanowells [3], nanodents [4], nanospikes [5,9], and hierarchical architecture [10] have been intensively investigated for the enhancement of light absorption. The enhancement is mainly attributed to the effective refractive index gradient from the top of the nano-structure to the bulk material and the increased optical path length created by structural scattering [11]. In addition to the geometry light trapping, novel designs exciting surface plasmon resonance [12] and photonic waveguide mode coupling [13] have been demonstrated to substantially improve the electromagnetic field in the absorber layers with enhanced light harvesting capability and thereafter photo-to-electric conversion efficiency.

We have recently demonstrated plasmonic back reflector through patterning aluminum foils by a series of electrochemical processes [4]. Thin-film amorphous silicon (a -Si:H) solar cells were constructed on the novel substrate and showed superior light capturing capability. Due to the nano-patterned surface, electrical parameters, such as electric field intensity, carrier density, recombination rate and current density, are supposed to be distributed in an uneven manner in microscopic inheriting the light absorption profile and device morphology. All these parameters will couple in a much more complicated way and make the overall energy conversion performance unpredictable. There is still a lack of fundamental understanding on the spatial distribution of these electrical parameters in nanostructured solar cells, which will couple in a rather complicated way and make the overall energy conversion performance unpredictable.

Optical simulations could reveal non-uniform light absorption profiles and coupling effects induced by the nanoscaled architectures. Using coupled optical and electrical modeling, Deceglie et al. [14] investigated the coupling effect of optical generation rate distribution and doping profiles, and pointed out that maximizing absorption in the intrinsic region rather than doped layers of thin film a -Si:H solar cells can provide an improved carrier collection and overall efficiency. In this work, simulations of coupled optical and electrical modeling are carried out based on thin-film n - i - p a -Si:H solar cells with nanodent array back reflector that has been experimentally realized in our previous work [4]. Full-wave electromagnetic simulations from the finite difference time domain (FDTD)

method are conducted to deduce the white-light optical generation rate. The carrier generation profiles in the a -Si:H layers were used as input, by interpolation, in a technology computer aided design (TCAD) device electrical simulation. The optical and electrical characteristics are studied by analyzing the coupling of non-uniformly distributed optical generation, electric field, carrier density, recombination, etc. These investigations have not only exemplified the critical necessity of the coupled optical/electrical design but also raised a set of generic guidelines for device performance optimization.

Theory and calculation

The closed-packed hexagonal nanodent structures formed on high purity Al foils (Figure 1a) are employed as the substrates. Experimentally, the pattern and pitch size can be controlled by the electrochemical process [4]. In this study, the pitch size defined by the distance between centers of two adjacent nanodents is around 500 nm. Thin-film n - i - p a -Si:H solar cells are constructed on this pre-patterned substrate as shown in Figure 1b. One dimensional (1-D) simulations have been used to provide valuable guidance for optimization of solar cell designs [15]. However, in order to accurately disclose the correlations of optical and electrical distribution in 3-D configuration, multi-dimensional simulations become crucially necessary. In our study, optical properties of the nanostructured solar cells were studied through 3-D optical simulation while electrical transport characteristics were calculated by 2-D manner to save computational resources. Meanwhile, a set of 2-D cross sections of structure were simulated to animate the electrical performances in three dimensions.

The 3-D structure of n - i - p a -Si:H solar cell used for the simulations is illustrated in Figure 1c by assuming conformal coating of each functional layer. The pitch size is set as 500 nm following the previous experimental results [4]. The corresponding thicknesses of each layer (Ag/TCO (transparent conductive oxide)/ n - a -Si:H/ i - a -Si:H/ p - a -Si:H/TCO) are set to be 100/30/20/200/10/80 nm, respectively. Figure 1d depicts the top view of the solar cell, where the rectangular area indicates one unit cell of the periodic structure. For comparison, planar solar cells with identical thickness of each layer are also investigated as control device.

The optical properties are simulated by numerically solving Maxwell's equations through a commercial FDTD simulation package [16]. In brief, a plane wave light source is set to be polarized along the x -axis, with symmetrical boundaries in the z -axis, anti-symmetrical boundaries in the x -axis, and perfectly matched layer (PML) boundary in the

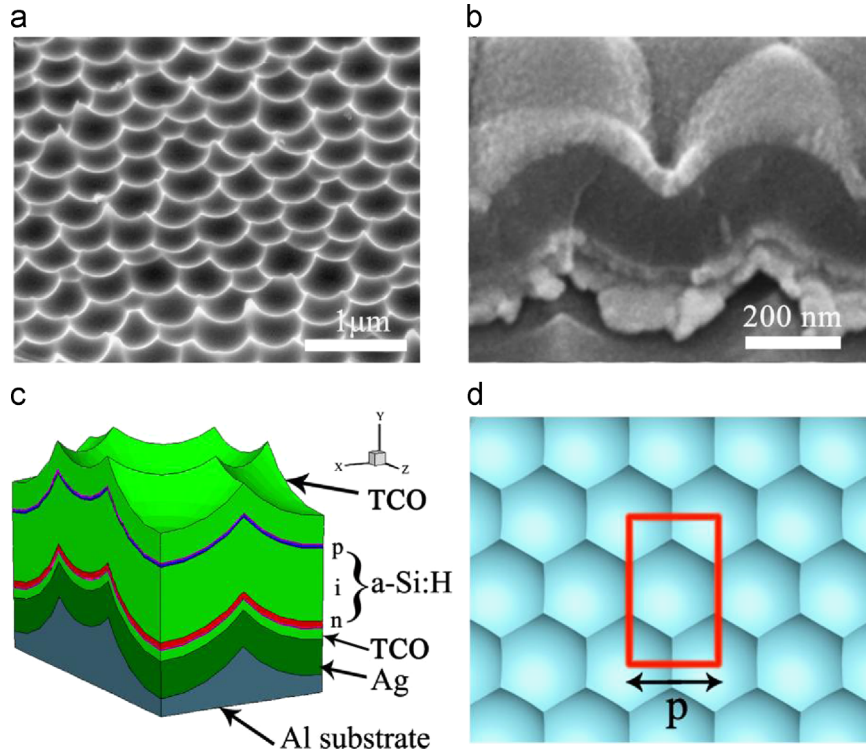


Figure 1 SEM images of the tilted views of (a) pre-patterned Al substrate and (b) corresponding *a*-Si:H solar cell. (c) A 3-D configuration of the unit cell used in the simulation. (d) Top view of the modeling device (pitch size (p)=500 nm). The labeled rectangle indicates the region of unit cell.

y-axis. Another orthogonally polarized light source along the *z*-axis is considered in parallel with symmetrical and anti-symmetrical boundaries along the *x*- and *z*-axes, respectively. The calculated optical generation rates under the two orthogonally polarized light sources will be averaged to imitate the incident sunlight [17, 18]. Optical data of Al and Ag are taken from Palik's Handbook of Optical Constants [19], and TCO and *n-i-p a-Si:H* layers are modeled using the measured data as described in our previous work [4].

The optical generation rate $G_{\text{opt}}(\lambda)$ of each wavelength can be calculated by using [20]

$$G_{\text{opt}}(\lambda) = \frac{\epsilon'' |\epsilon(\lambda)|^2}{2\hbar} \quad (1)$$

where ϵ'' is the imaginary part of material permittivity, \hbar is Planck's constant divided by 2π , $|\epsilon(\lambda)|^2$ is the wavelength dependent on optical field intensity. The optical generation rate profiles at each wavelength (11.1 nm interval in 0.3–1.4 μm wavelength range) weighted by the standard air mass (AM) 1.5 spectrum are integrated to get white-light profiles. The white-light optical generation rate profiles in *n-i-p a-Si:H* layers act as the input.

2-D simulations are carried out in the subsequent electrical simulations by using Synopsys Sentaurus TCAD suite while assuming ideal ohmic contacts imposed on vertical boundaries. Neumann boundary conditions are employed to model the periodic geometry in horizontal directions that are not defined as the contacts [21]. It is known that the disordered characteristic of *a-Si:H* results in a continuous density of states (DOS) within the localized states as a function of energy. The localized states of amorphous silicon can be expressed by dangling defect states, and the tails of

conduction band (CB) and valence band (VB) [22]. The defect states within the bandgap could follow Gaussian profiles while the band tails can be represented by exponential function [23]. A set of parameters for depicting these states and other electrical properties are adopted from literature [24] as listed in the Supporting Information (Table. S1). The electric field is calculated by Poisson's equation [25]:

$$\nabla \cdot \vec{E} = \frac{q}{\epsilon} \rho \quad (2)$$

where \vec{E} is the electric field, q is the elementary charge, ϵ is the material permittivity and ρ is the space charge density.

The current density profile and *J-V* curve are calculated by solving electron (Eq. (3)) and hole (Eq. (4)) continuity equations [26]:

$$\nabla \cdot \vec{J}_n = q(G - R) + q \frac{\partial n}{\partial t} \quad (3)$$

$$-\nabla \cdot \vec{J}_p = q(G - R) + q \frac{\partial p}{\partial t} \quad (4)$$

in which \vec{J}_n and \vec{J}_p are the electron and hole current densities, respectively, R is the recombination rate, n and p are the densities of holes and electrons, respectively; and the transport equations for electron (Eq. (5)) and hole (Eq. (6)) [26]

$$\vec{J}_n = q\mu_n n \vec{E} + qD_n \nabla n \quad (5)$$

$$\vec{J}_p = q\mu_p p \vec{E} - qD_p \nabla p \quad (6)$$

in which μ_n and μ_p are the electron and hole mobilities, respectively, D_n and D_p are the electron and hole diffusion coefficients, respectively.

Results and discussion

Figure 2a shows the optical generation rate profile in a planar device, while the profile along the cross section (as indicated by the central black dash line in Figure 2d) is presented in Figure 2b. The corresponding 1-D generation rate profiles vertically along the guidelines are displayed in Figure 2c. In the case of planar device, the maximum value appears at the top of the α -Si:H layer and decreases steadily as the light passes through the active layer. The broad peak centered at 146 nm apart from top layer arises from the interference effect in planar configuration. In comparison, the solar cell on nanopatterned substrate shows greatly enhanced generation rate, with an irregular but symmetrical shape arising from the periodic geometry as indicated in Figure 2b. Relatively higher values are distributed along the y -axis at $x=0$, and the front parts near horizontal boundaries (*i.e.* two top corners). Meanwhile, the relatively lower generation rate regions exist, which symmetrically locate around the median (light blue region). The improved overall optical performance is ascribed to the efficient scattering of light in the short wavelength region and the excitation of surface plasmon polaritons (SPP) modes, localized surface plasmon (LSP) resonances and waveguide modes in long wavelength region as explicated in the previous report [4].

For the patterned solar cell, the understanding of the complex internal field (*i.e.* electric field and current density)

profiles has become imperative to predict and optimize device efficiency. The following 2-D numerical simulations that describe the transport processes are carried out on one representative cross section as illustrated by the dashed black line in the inset in Figure 2d. Electric field profiles are calculated by solving Poisson's equation (Eq. (2)). In the planar solar cell under 0 V bias voltage, as shown in Figure 3a, the electric field intensity shows very high values at the p/i and i/n interfaces and exhibits approximately uniform distribution within i -layer. This is in agreement with the experimental results measured by scanning Kelvin probe microscopy [27]. While for the patterned solar cell (Figure 3b), the central region near the top of intrinsic layer and the regions around the coordinate of $(\pm 0.25, 0.06)$ present higher electric field strength than that in other regions. The corresponding 1-D electric field profiles (Figure 3c) along the guided lines in Figure 3a and b further state out the field characteristics for the planar and patterned solar cells, respectively.

The current density can be deduced by numerically solving the Poisson equation, continuity equations, and transport equations on the finite element mesh with respect to AM1.5G spectrum [26]. Subsequently, quasi-statically sweeping the voltage boundary conditions at the contacts can obtain white-light current density-voltage (J - V) curves. Taking the complex 3-D configuration into account with the non-uniform distributions of generation and recombination rates, J - V curves are calculated from ten different cross section traces with interval of 40-50 nm. The electrical properties obtained from ten J - V curves and three representative results can be found in Figure 2d and also listed in Table. S2 (Supporting Information). The patterned solar cell presents improvements of 32% in short circuit current (J_{sc})

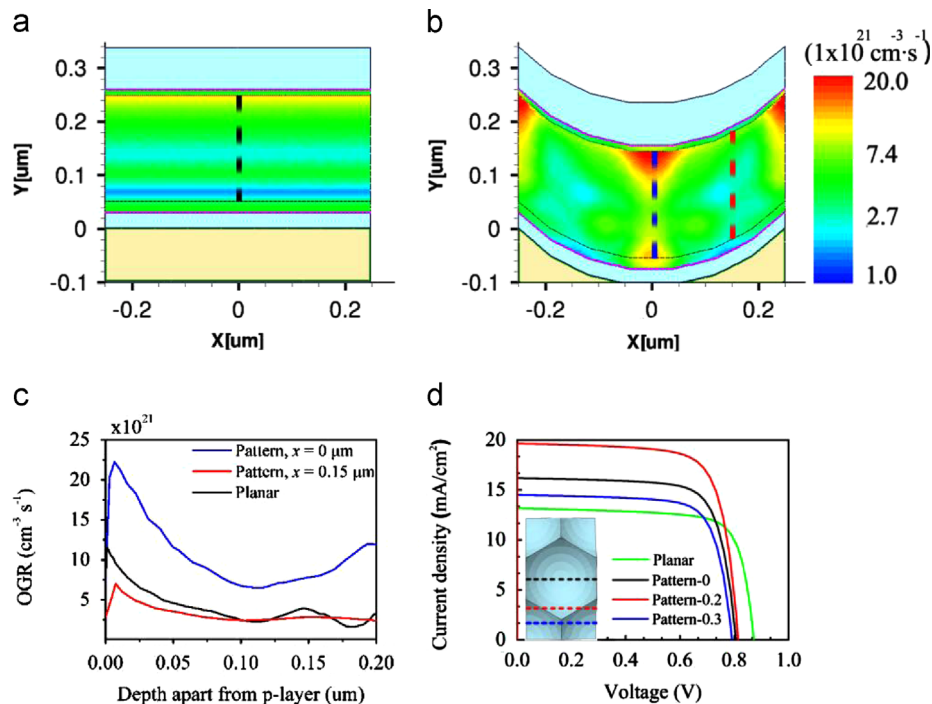


Figure 2 2-D generation rate distributions in α -Si:H layers with (a) planar and (b) textured configurations. (c) 1-D generation rate profiles in the intrinsic silicon layer with respect to the corresponding guideline in (a) and (b). (d) J - V curves of planar (green) and patterned (black, red and blue lines) solar cells calculated from 2-D cross sections. The corresponding simulation cross sections are labeled in the inset figure. Pattern-0.2 and pattern-0.3 indicate the cross section with 0.2 and 0.3 μm apart from the central black dash line.

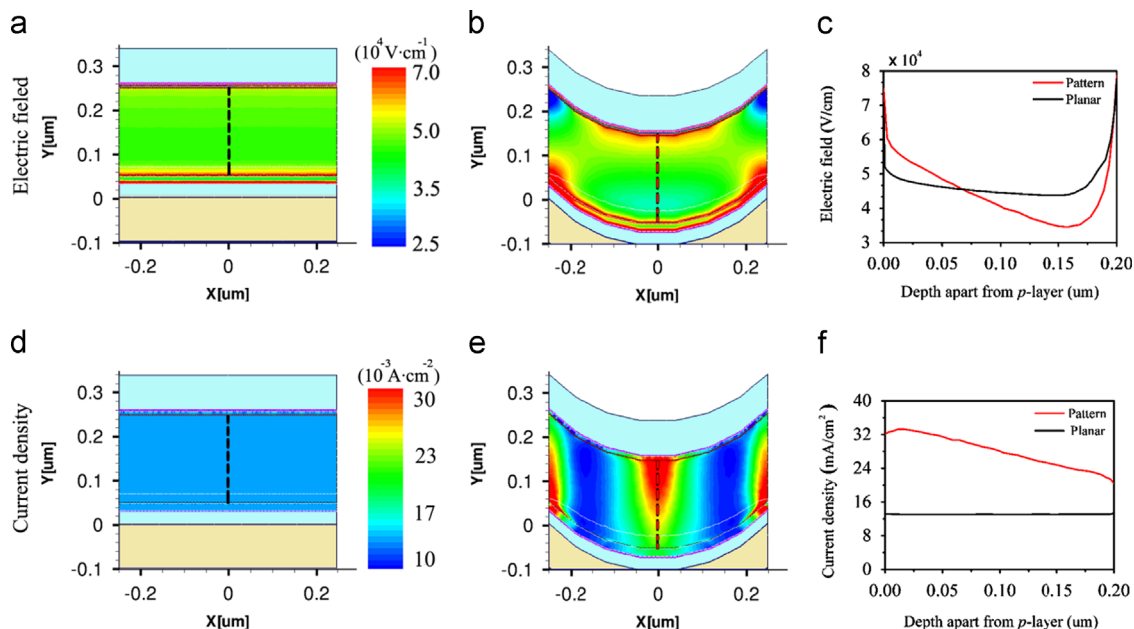


Figure 3 (a-c) Electric field and (d-f) current density profiles in (a, d) planar and (b, e) patterned solar cells, respectively. (c, f) The 1-D profiles in the intrinsic silicon layer with respect to the corresponding guidelines. Bias voltage = 0 V.

and 27% in energy conversion efficiency (ζ), which mainly benefit from the effective optical management. However, it is clearly seen that patterned device has lower average open circuit voltage (0.799 V) than planar device (0.827 V) that will be discussed in the later sections.

Figure 3d-f shows the current density profiles of the planar device and patterned device. The planar solar cell shows uniform current density across the active layer which is 200 nm in thickness while patterned solar cell possesses symmetric higher current density as displayed in red in Figure 3e. Careful observation in Figures 3b, e and 2b discloses that the regions with high generation rate and strong electric field intensity are preferable to possess high current density.

While the patterned solar cell provides higher current density as compared with planar device, a decrease of V_{OC} is usually observed. This result is in contrast to the recent results from both simulation and experiments [14,28], that V_{OC} is improved due to increased photocurrent. Normally, there are two possible reasons that could lead to the reduction of V_{OC} , e.g. increased junction area and deviations from conformal coating with degraded material quality on the highly textured substrate [29-32]. In case of a -Si:H solar cells, the trap-mediated recombination in the bulk rather than the forward bias current injected across the diode junction plays the major role [33-35]. Moreover, in our device modeling, it is assumed that each functional layer is conformally coated with uniform film quality without variation. As a result, the above two reasons on V_{OC} reduction are not valid.

The variation of V_{OC} could originate from the different optoelectrical spatial distributions in the planar and patterned solar cells. To verify the assumption, the electric field and current density distributions are calculated under different bias voltages as shown in Figure 4, where the white triangles indicate the flow direction of current and electric field.

In contrast to the uniform distribution laterally in planar cells (Figure 4a), the patterned solar cell exhibits non-uniformity of

electric field, where the suppressed regions can be found at top corners as labeled in Figure 4b. As the bias voltage increases to 0.8 V, the suppressed electric field strength located at the same region becomes much distinct (Figure 4f). The current density distribution in planar device stays uniform (Figure 4c and g) while the patterned device shows symmetric distribution feature as shown in Figure 4d and h. Detailed observation indicates that the external bias voltage (0.8 V, $V_{OC}=0.806$ V) induces a localized current reversal in the both sides of unit cell (Figure 4h) and net photocurrent approaching zero. The spatial distributions of current density with the bias voltage ranging from 0.75 to 1.0 V are also elucidated in Figure S1. Further increased bias voltage at 0.85 V yields complete inversion as can be seen in Figure S1e.

Spatial field analysis suggests that the current density distributions are closely related with geometric shape of solar cell. Meanwhile, the predominated transport in a -Si:H solar cells is governed by drift collection [36,37]. The internal electric field plays a vital role to enhance the drift current while restrain the diffusion current flow from p to n layer [38,39]. The regions with different electric fields can be considered as sub-cells that compose the whole solar cell in parallel or series configurations. The weaker electric field regions are preferred for the initiation of current reverse under a forward bias, and in turn are responsible for the decrease of V_{OC} . Thus the V_{OC} of the patterned cell mainly depends on the regions with the lowest electric field. This microscopic current reversal explains why the V_{OC} of the patterned solar cells is lower than that of planar solar cells although the patterned solar cell has a higher J_{SC} under the condition that p -layer doping concentration is $3 \times 10^{18} \text{ cm}^{-3}$.

In a -Si:H solar cells, one strategy to achieve a higher V_{OC} is to raise the internal electric field by increasing the doping concentration. Consequently, a higher p -layer doping concentration of $8 \times 10^{18} \text{ cm}^{-3}$ is used to investigate the V_{OC} variation and fields profiles in microscopic scale. Figure 5a indicates that higher doping concentration of p layer leads

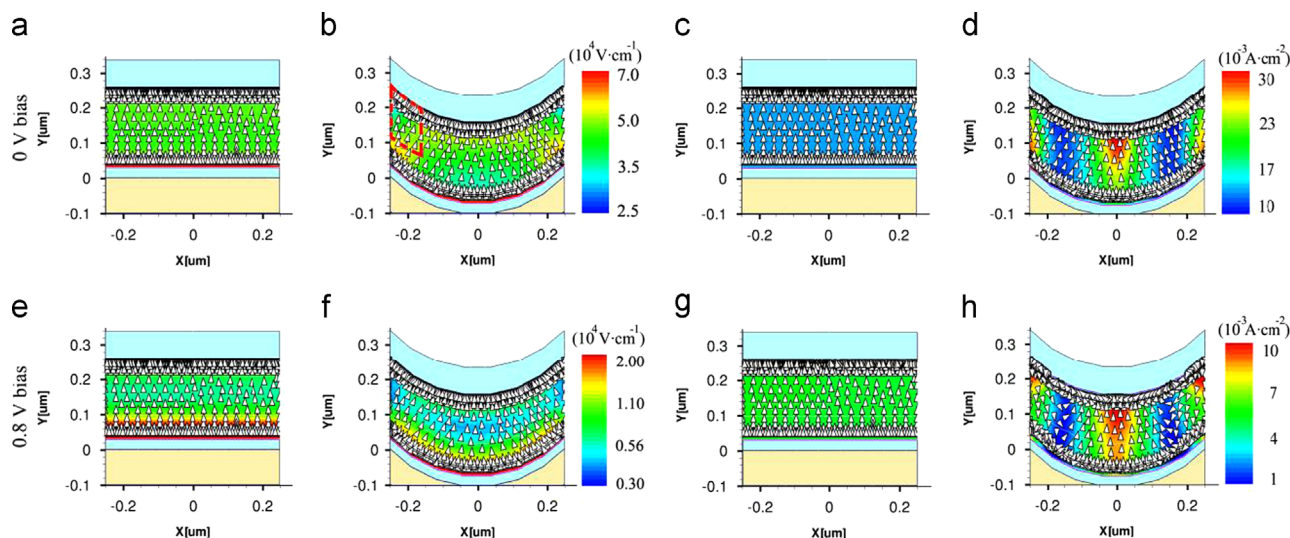


Figure 4 (a, b, e, f) Electric field and (c, d, g, h) current density profiles of (a, c, e, g) planar and (b, d, f, h) nanopatterned solar cells under (a-d) 0 V and (e-h) 0.8 V forward bias (p -layer doping concentration: $3 \times 10^{18} \text{ cm}^{-3}$). The arrows in the above corresponding figures indicate the directions of electric field and the current density.

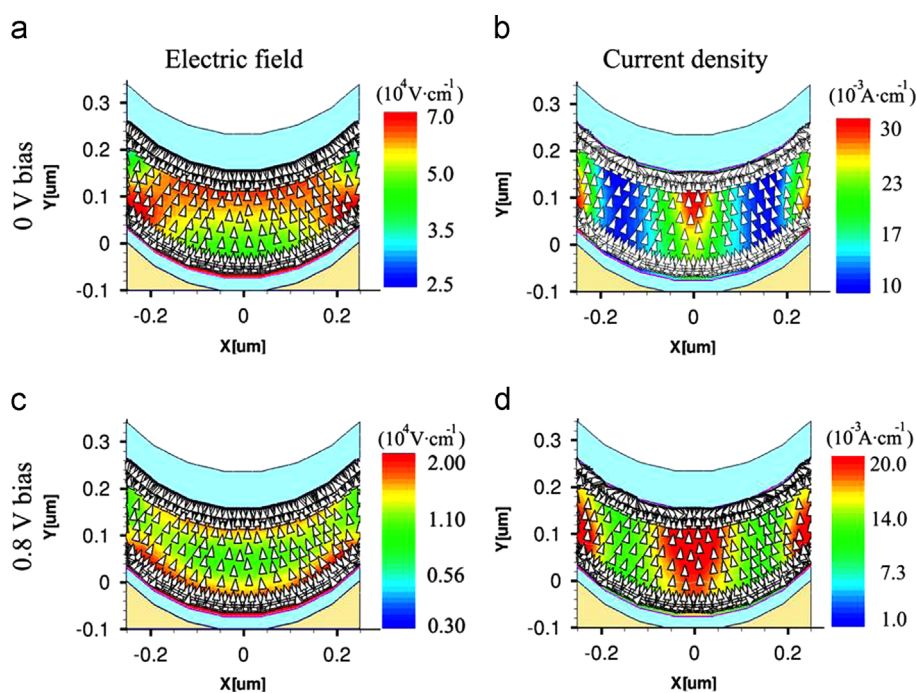


Figure 5 Spatial distribution of electric field (a and c) and current density (b and d) under 0 V bias (a and b) and 0.8 V bias (c and d). p -Layer doping concentration: $8 \times 10^{18} \text{ cm}^{-3}$.

to a broader and higher internal electric field region, although the relatively lower internal electric field regions still exist. The overall electric field is suppressed by increasing the bias voltage imposed upon the contact (Figure 5c and Figure S1), however it is still stronger than the device with lower doping concentration at the same bias voltage (Figure 4f and Figure S1). Comparing Figures 4h and 5d, there is no current reversal in higher doping concentration device at the corresponding regions under 0.8 V bias voltage. The curvature weakened local electric field is now not significant enough to cause the current reversal under

higher doping concentration. Although the current reverse will be eventually launched above 0.9 V (see Figure S1h and j) at the top corners by further increasing the positive bias voltage, the increase of p -layer doping concentration is evidently an efficient approach to improve the V_{OC} and photo-electric conversion efficiency.

In addition to the electric field and current density, it is of interest to see the variation of solar cell performance under different doping concentrations. Figure 6 shows the performance parameters of both planar and patterned devices as a function of p -layer doping concentration where the optical

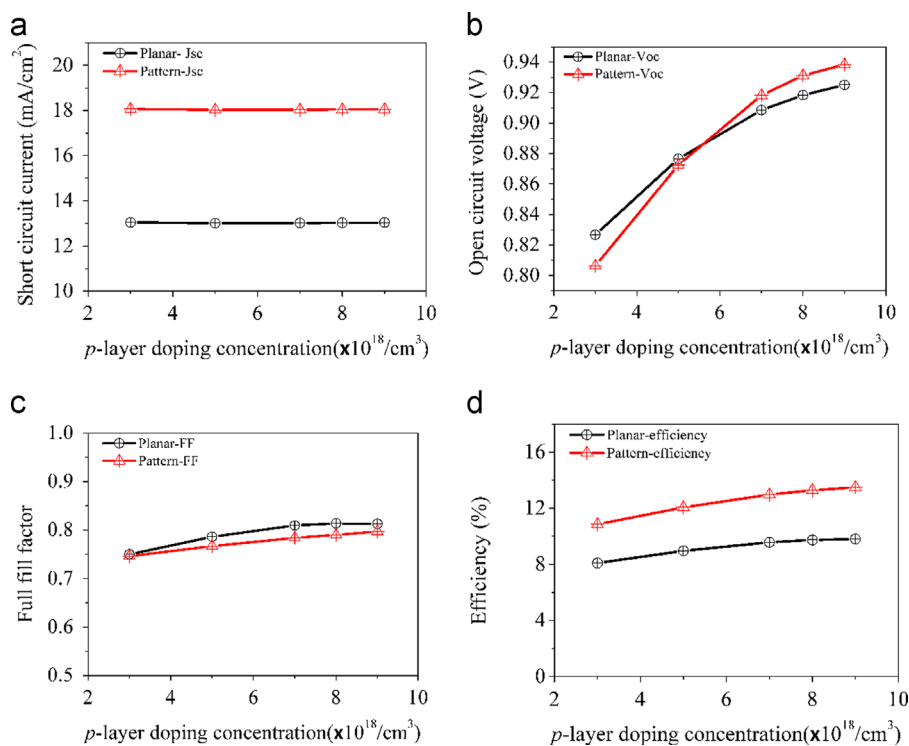


Figure 6 The dependences of (a) short circuit current J_{SC} , (b) open circuit voltage V_{OC} , (c) fill factor FF and (d) solar cell efficiency on p -layer doping concentration.

properties are assumed to be independent to doping concentration. Patterned devices hold higher short circuit current due to the superior light harvesting capability (Figure 6a). With the increase of p -layer doping concentration, the V_{OC} of patterned solar cell increases dramatically and surpasses the planar ones at the doping concentration of $7 \times 10^{18} \text{ cm}^{-3}$ in Figure 6b. Figure 6c shows that both devices have increasing fill factors (FFs), which could be contributed by the enhanced carrier separation due to the increasing internal electric field. Finally, the efficiency has positive correction to increasing p -layer doping concentration where the patterned solar cell achieves an efficiency up to 13.496% with a 38% improvement compared with that of planar device (see Figure 6d).

Conclusions

The optical and electrical performances of thin film a -Si:H solar cells based on hexagonal patterned back reflector are evaluated by numerical simulations. The patterned solar cell illustrates an outstanding optical absorption enhancement compared with planar solar cell. The regions of high optical generation rate and strong electric field account for the high current density that greatly improves the performance of patterned solar cell. Meanwhile, due to the non-uniform electric field distribution, weaker internal electric field region causes localized current reversal when the forward bias voltage approaches V_{OC} . Increasing the doping concentration in doped layer yields enhanced internal electric field, which can effectively improve the V_{OC} and eventually photo-electric conversion efficiency of patterned solar cells. By employing the patterned solar cell, this study based on optically and electrically coupled simulation method demonstrates a rational strategy to design

and optimize the nanostructured thin film solar cells as well as other optoelectronic devices.

Acknowledgments

This work was financially supported by the National Natural Science Foundation of China (61371016, 51102271, and 11174308), the Science & Technology Commission of Shanghai Municipality (Grant no. 13DZ1106000), and General Research Fund 612113 from the Hong Kong Research Grant Council.

Appendix A. Supporting information

Supplementary data associated with this article can be found in the online version at <http://dx.doi.org/10.1016/j.nanoen.2014.05.021>.

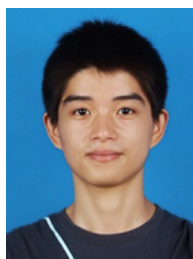
References

- [1] Z. Fan, H. Razavi, J.-w. Do, A. Moriwaki, O. Ergen, Y.-L. Chueh, P.W. Leu, J.C. Ho, T. Takahashi, L.A. Reichertz, S. Neale, K. Yu, M. Wu, J.W. Ager, A. Javey, *Nat. Mater.* 8 (2009) 648-653.
- [2] C. Battaglia, C.-M. Hsu, K. Söderström, J. Escarré, F.-J. Haug, M. Charrière, M. Boccard, M. Despeisse, D.T.L. Alexander, M. Antoni, Y. Cui, C. Ballif, *ACS Nano* 6 (2012) 2790-2797.
- [3] S.-F. Leung, M. Yu, Q. Lin, K. Kwon, K.-L. Ching, L. Gu, K. Yu, Z. Fan, *Nano Lett.* 12 (2012) 3682-3689.
- [4] H. Huang, L. Lu, J. Wang, J. Yang, S.-F. Leung, Y. Wang, D. Chen, X. Chen, G. Shen, D. Li, Z. Fan, *Energy Environ. Sci.* 6 (2013) 2965-2971.

- [5] R. Yu, K.-L. Ching, Q. Lin, S.-F. Leung, D. Arcrossito, Z. Fan, *ACS Nano* 5 (2011) 9291-9298.
- [6] J. Müller, B. Rech, J. Springer, M. Vanecek, *Sol. Energy* 77 (2004) 917-930.
- [7] C. Rockstuhl, S. Fahr, K. Bittkau, T. Beckers, R. Carius, F. J. Haug, T. Söderström, C. Ballif, F. Lederer, *Opt. Express* 18 (2010) A335-A341.
- [8] B. Wang, P.W. Leu, *Nanotechnology* 23 (2012) 194003.
- [9] S.-F. Leung, L. Gu, Q. Zhang, K.-H. Tsui, J.-M. Shieh, C.-H. Shen, T.-H. Hsiao, C.-H. Hsu, L. Lu, D. Li, Q. Lin, Z. Fan, *Sci. Rep.* 4 (2014) 4243.
- [10] H.-P. Wang, T.-Y. Lin, C.-W. Hsu, M.-L. Tsai, C.-H. Huang, W.-R. Wei, M.-Y. Huang, Y.-J. Chien, P.-C. Yang, C.-W. Liu, L.-J. Chou, J.-H. He, *ACS Nano* 7 (2013) 9325-9335.
- [11] M. Yu, Y.Z. Long, B. Sun, Z.Y. Fan, *Nanoscale* 4 (2012) 2783-2796.
- [12] H.A. Atwater, A. Polman, *Nat. Mater.* 9 (2010) 205-213.
- [13] G. Gomard, E. Drouard, X. Letartre, X.Q. Meng, A. Kaminski, A. Fave, M. Lemitte, E. Garcia-Caurel, C. Seassal, *J. Appl. Phys.* 108 (2010) 123102.
- [14] M.G. Deceglie, V.E. Ferry, A.P. Alivisatos, H.A. Atwater, *Nano Lett.* 12 (2012) 2894-2900.
- [15] M. Kabir, Z. Ibrahim, K. Sopian, N. Amin, *Sol. Energy Mater. Sol. Cells* 94 (2010) 1542-1545.
- [16] FDTD Solutions. (Cited 2013 February 4), Available from: <http://www.lumerical.com>.
- [17] S. Hu, C.-Y. Chi, K.T. Fountaine, M. Yao, H.A. Atwater, P. D. Dapkus, N.S. Lewis, C. Zhou, *Energy Environ. Sci.* (2013) 1879-1890.
- [18] M.G. Deceglie, V.E. Ferry, A.P. Alivisatos, H.A. Atwater, *IEEE J. Photovolt.* 3 (2013) 599-604.
- [19] E.D. Palik, *Handbook of Optical Constants of Solids: Index*, vol. 3, Access Online via Elsevier, 1998.
- [20] V.E. Ferry, M.A. Verschuuren, H.B.T. Li, E. Verhagen, R.J. Walters, R.E.I. Schropp, H.A. Atwater, A. Polman, in: *Proceedings of the 35th IEEE Photovoltaic Specialists Conference*, 2010, pp. 760-765.
- [21] TCAD Sentaurus. (Cited 2013 February 4), Available from: <http://www.synopsys.com>.
- [22] R.A. Street, *Hydrogenated Amorphous Silicon*, Cambridge University Press, New York, 2005.
- [23] M. Zeman, J. Krc, Electrical and optical modelling of thin-film silicon solar cells. In: *Proceedings of MRS*, V. Chu, S. Miyazaki, A. Nathan, J. Yang, H.W. Zan, (Eds.), Cambridge University Press, San Francisco, California, 2007.
- [24] M.Z. Ruud, E.I. Schropp, *Amorphous and Microcrystalline Silicon Solar Cells: Modeling, Materials and Device Technology*, Springer-Verlag, New York, LLC232.
- [25] N. Palit, U. Dutta, P. Chatterjee, *Indian J. Phys.* 80 (2006) 11-35.
- [26] M. Hack, *M. Shur*, *J. Appl. Phys.* 58 (1985) 997-1020.
- [27] C.S. Jiang, H.R. Moutinho, M.J. Romero, M.M. Al-Jassim, Y. Q. Xu, Q. Wang, *Thin Solid Films* 472 (2005) 203-207.
- [28] V.E. Ferry, M.A. Verschuuren, M.C.v. Lare, R.E. Schropp, H. A. Atwater, A. Polman, *Nano Lett.* 11 (2011) 4239-4245.
- [29] C.M. Hsu, C. Battaglia, C. Pahud, Z.C. Ruan, F.J. Haug, S. H. Fan, C. Ballif, Y. Cui, *Adv. Energy Mater.* 2 (2012) 628-633.
- [30] H.B.T. Li, R.H. Franken, J.K. Rath, R.E.I. Schropp, *Sol. Energy Mater. Sol. Cells* 93 (2009) 338-349.
- [31] M. Tang, S.T. Chang, T.C. Chen, Z.W. Pei, W.C. Wang, J. Huang, *Thin Solid Films* 518 (2010) S259-S261.
- [32] H. Sakai, T. Yoshida, T. Hama, Y. Ichikawa, *Jpn. J. Appl. Phys.* 29 (1990) 630-635.
- [33] M.G. Deceglie, V.E. Ferry, A.P. Alivisatos, H.A. Atwater, *Nano Lett.* 12 (2012) 2894-2900.
- [34] S.W. Boettcher, J.M. Spurgeon, M.C. Putnam, E.L. Warren, D. B. Turner-Evans, M.D. Kelzenberg, J.R. Maiolo, H.A. Atwater, N.S. Lewis, *Science* 327 (2010) 185-187.
- [35] B.M. Kayes, H.A. Atwater, N.S. Lewis, *J. Appl. Phys.* 97 (2005) 114302.
- [36] A. Shah, J. Meier, E. Vallat-Sauvain, N. Wyrsh, U. Kroll, C. Droz, U. Graf, *Sol. Energy Mater. Sol. Cells* 78 (2003) 469-491.
- [37] J. Meier, R. Fluckiger, H. Keppner, A. Shah, *Appl. Phys. Lett.* 65 (1994) 860-862.
- [38] L.J.A. Koster, E.C.P. Smits, V.D. Mihailetschi, P.W.M. Blom, *Phys. Rev. B* 72 (2005) 085205.
- [39] J. Furlan, *Prog. Quant. Electron.* 25 (2001) 55-96.



Ruichao Guo is currently a joint graduate student of Huazhong University of Science and Technology (HUST) and Shanghai Advanced Research Institute (SARI), Chinese Academy of Sciences for master's degree. His current scientific interest focuses on optical and electrical simulations of nanostructured optoelectronic devices.



Hongtao Huang is currently a joint Ph.D. candidate of Huazhong University of Science and Technology (HUST) and Shanghai Advanced Research Institute (SARI), Chinese Academy of Sciences. His current scientific interests are optoelectronic thin film materials and devices.



Paichun Chang received his M.S degree of Electrical Engineering in 2004 and Ph.D. degree of Materials Science Engineering in 2008 from University of California, Irvine. He was a postdoctoral fellow in University of Southern California during 2009 and 2010, and worked on metallic nanowire sensor and nanowire based energy applications. He is an assistant professor in Kainan University, Taiwan. His research field includes surface treatments, 3D printing, and functionalized nanomaterials.



Linfeng Lu received his Ph.D. degree in Material Science from the Nanjing University of Aeronautics and Astronautics, in 2010. Currently, he worked at Shanghai Advanced Research Institute, Chinese Academy of Sciences. His research focuses on semiconductor thin films for technological applications in photovoltaic devices.

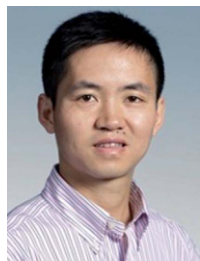


Xiaoyuan Chen received a Ph.D. from the University of Strathclyde, UK in 1991 and has worked in both academia (Massachusetts Institute of Technology, University of Iowa, University of Cardiff, and industry (Corning) on semiconductor physics and devices. He joined the faculty at Shanghai Advanced Research Institute, Chinese Academy of Sciences in 2010. His research interests focused on photon, phonon and

electron interactions in low-dimensional structures, and optoelectronic, and thermoelectric device application of these structures.



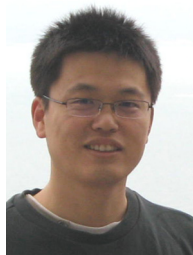
Xiaofei Yang received his Ph.D. degree from the Department of Electronic Science and Technology at Huazhong University of Science and Technology, China, in 1999. He is currently a Professor in the School of Optical and Electronic Information at Huazhong University of Science and Technology. His research interests focus on smart materials and intelligent system.



Zhiyong Fan received his Ph.D. degree from the University of California, Irvine, in 2006 in Materials Science. From 2007 to 2010 he worked at the University of California, Berkeley, as a postdoctoral fellow in the department of Electrical Engineering and Computer Sciences, with a joint appointment with Lawrence Berkeley National Laboratory. In May 2010, he joined the Hong Kong University of Science and Technology as an assistant professor. His research interests include engineering novel nanostructures with functional materials for technological applications including energy conservation, electronics and sensors, etc.



Benpeng Zhu was a joint Ph.D. student of the Department of Biomedical Engineering at University of Southern California, Los Angeles, CA, and School of Physics and Technology at Wuhan University, China, and received his Ph.D. degree in 2009. He currently works as an Associate Professor in the School of Optical and Electronic Information at Huazhong University of Science and Technology. His research interests include the development of electronic ceramics, films and composites, as well as fabrication of functional device.



Dongdong Li received his Ph.D. degree in Materials Science from Shanghai Jiao Tong University in 2010. Under the support of Ministry of Education of the People's Republic of China, he worked in the Department of Electrical Engineering at the University of Southern California (2007-2009). Currently, he is an associate professor at Shanghai Advanced Research Institute, Chinese Academy of Sciences. His research focuses on structural and interfacial engineering of functional nanomaterials, for technological applications in energy conversion and storage.